Journal of Molecular Graphics and Modelling 87 (2019) 185–191

Contents lists available at ScienceDirect

Journal of Molecular Graphics and Modelling

journal homepage: www.elsevier.com/locate/JMGM

Influence of the T to S mutation at the STMK motif on antibiotic resistance of penicillin binding protein 1A: A comprehensive computational study

Esmaeil Behmard [a, b], Ali Ahmadi [a, *], Ali Najafi [a]

[a] Molecular Biology Research Center, Systems Biology and Poisonings Institute, Baqiyatallah University of Medical Sciences, Tehran, Iran
[b] The School of Advanced Medical Sciences and Technologies, Fasa University of Medical Sciences, Fasa, Iran

ARTICLE INFO

Article history:
Received 24 August 2018
Received in revised form
13 November 2018
Accepted 4 December 2018
Available online 7 December 2018

Keywords:
Penicillin binding protein 1A
β-Lactam antibiotic
Antibiotic resistance
Umbrella sampling
MD simulations

ABSTRACT

The emergence of antibiotic resistance has attracted the attention of scientists and scientific circles over the decades. β-Lactam antibiotics resistance is a worldwide therapeutic challenge in bacterial infections, mediated through several mechanisms of which mutations in Penicillin Binding Proteins (PBPs) are an important issue, making critical therapeutic problems in the human population. Accordingly, investigating the dynamic structures of mutant variants could result in a profound understanding of such a specific resistance. Therefore, this work investigated structural properties sampled by all-atom molecular dynamics (MD) simulations, umbrella sampling, and binding free energy calculations for both a wild-type and a cefotaxime-resistant T to S mutant of PBP1A. The T to S mutation significantly reduces the binding affinity of cefotaxime (a frequently clinically-administrated β-lactam antibiotic) as the PBP1A inhibitor. In the conventional MD simulations presented here, more fluctuations of the mutant's active site cleft margins were detected. The cleft of the mutant protein also opened remarkably more than the wild-type's cleft and displayed more flexibility. Thus, our findings have shown that flexibility of cleft margins of the active site in the mutant PBP1A immediately results in the catalytic cleft opening. In addition, binding free energy calculation suggests that reducing hydrophobic contacts and increasing the polar contribution in the binding energy may play an important role in cefotaxime resistance.

1. Introduction

For over five decades, β-lactam antibiotics, including penicillins and cephalosporins, have been widely applied for the treatment of bacterial infections [1]. The target proteins for β-lactam drugs are multiple specific proteins named penicillin-binding proteins (PBPs) that operate in the last step of bacterial cell wall synthesis [2,3]. The β-lactam antibiotics inhibit PBPs by acetylating the hydroxyl element in the catalytic site of PBPs in a reaction similar to that of their activity [4,5].

By reducing the success of available therapeutic regimens in various bacteria, and increasing the risk of spreading multiple antibiotic resistant pathogens, antibiotic resistance has become one of the most dangerous threats to public health. Resistance to β-lactam antibiotics can occur via several mechanisms [6,7]. Some bacteria produce beta-lactamase enzymes that inactivate and destroy antibiotics by cutting key bonds [6,7]. Some other mechanisms depend on the activity of efflux pumps that exhaust drugs from intracellular space, reducing the concentration of antibiotics in the periplasmic space of Gram-negative bacteria [7–9]. Studies have also reported that mutations in key structural motifs of PBP1A significantly reduce its sensitivity to antibiotics [10,11], in which some specific conserved motifs mutations especially in the C-terminal and transpeptidase (TP) regions [10,11], are responsible for high-level resistances to β-lactam antibiotics [10–12]. 3D structural investigations have demonstrated that PBPs contain a catalytic cleft located within an elongated, highly hydrophobic, tunnel-like zone, with three major motifs in the active central part [13,14], including: SXXK (S370–T371–M372-K373), which contains the catalytic serine located at the amino-terminal of α2, SXN (S428–R429–N430) located on a loop between α4 and α5, and KTG (557–559) at the carboxyl-terminal of β3 [13,14]. Many

* Corresponding author. Medical Bacteriology, Molecular Biology Research Center, Systems Biology and Poisonings Institute, Baqiyatallah University of Medical Sciences, Vanak avenue, Mollasadra street, BMSU, Tehran, Iran.
E-mail address: aliahmadi@bmsu.ac.ir (A. Ahmadi).

https://doi.org/10.1016/j.jmgm.2018.12.002
1093-3263/

epidemiological studies have shown that a single mutation, T371A or S in the SXXK motif, is conserved among a variety of strains, and has a significant effect on the affinity of PBP1A to β-lactams [13,14]. How such a low tendency can eliminate the lethal effect of β-lactams, and at the same time, maintains the activity of PBPs is under debates for many years. To better understand the molecular details of T to S mutation at the SXXK motif, in the present study, we examined the structural and dynamical effects of the T to S mutation in the context of both wild-type and mutant PBP1A variants, on the binding of cefotaxime, a third generation cephalosporin.

2. Material and methods

2.1. Protein structure preparation and molecular docking

UniProt Knowledge Base (primary accession no. A0A1D8GR86) was used to extract the PBP1A sequence from *S. pneumonia*. This sequence was accepted as an input to search homologous protein structures using Optimized Protein Fold RecognitION (ORION) online web server [15]. The PBP1A from *S. pneumonia* (PDB ID: 2V2F) was selected as the appropriate structural template [14]. The template structure has the query coverage, percentage of identity, and structural resolution of 91.69%, 88.31%, and 1.9 Å, respectively. Moreover, ORION web server was used to perform sequence alignment. Finally, the DOPE score was utilized to select the best structure. Also, VERIFY-3D, ERRAT, Ramachandran map and ProSA were used to evaluate the quality of the best structure. The evaluation results showed that the model made by Modeller 9.14 was the best model with 97% of residues in the favored zone of the Ramachandran map, 91.14% ERRAT, and 88.82% VERIFY-3D scores (Fig. S1). Moreover, the ProSA Z-score showed that the best model has a good quality (Fig. S1). Therefore, it can be suggested that the built model is reliable. DrugBank was used to extract the three-dimensional structure of cefotaxime. PBP1A and cefotaxime parameter files were prepared using AutoDockTools-1.4.5 [16]. Autodock Vina package was utilized to provide the molecular docking of cefotaxime with PBP1A with all ligand torsions set flexible [17]. Then, the conventional MD simulations were initiated by the best complex of docking's output for both systems.

2.2. Molecular dynamic simulation

Conventional molecular dynamics simulations of the proteins in complex with an antibiotic, were performed using GROMACS 4.6.4. The proteins were modeled by the GROMOS96 (53a6) force field. Cefotaxime was modeled using the Topolbuild, developed by Bruce D. Ray. Then, each complex was solvated in the TIP3P water cubic box. Next, the proper number of solvent molecules were replaced with the ions to keep the whole system neutral. The whole system was minimized by steepest descent algorithm for 50,000 steps. Then, each system was gradually heated from 273 K to 310 K for 0.5 ns in the NVT ensemble. Conformations were stored every 0.01 ns with a time step of 2 fs in the NPT ensemble ($T = 310$ K and $P = 1$ atm). The SHAKE algorithm was applied to constrain the internal degrees of freedom of the water molecules, the particle mesh Ewald was applied to consider long-range electrostatic contacts, and the LINCS procedure was used to restrain all bond lengths in the proteins molecules, for both systems during simulations. Eventually, all production runs were done for 50 ns at 310 K [18–20]. The Gromacs toolbox, PyMol [21], and LigPlot [22] tools were used to analyze the simulation trajectories.

2.3. Free energy calculations

First of all, for assessment of the binding free energies using the MM/GBSA procedure, 500 conformations were selected from the last 10 ns AMBER simulation frames at intervals of 0.02 nm. Then, the MM/GBSA method was applied to calculate the binding free energy using the following equations:

$$\Delta G_{bind} = G_{complex} - (G_{protein} + G_{ligand})$$

$$\Delta G_{bind=} \Delta E_{MM} + \Delta G_{solv} - T\Delta S$$

$$= \Delta E_{vdW} + \Delta E_{ele} + \Delta G_{pol} + \Delta G_{nonpol} - T\Delta S$$

In these equations $G_{complex}$, G_{ligand}, and $G_{protein}$ indicate free energies of the complex, ligand, and receptor, respectively. A sum of changes in molecular mechanical (MM) gas-phase binding energy (ΔE_{MM}), the solvation free energy (ΔG_{solv}), and entropic ($-T\Delta S$) contributions were applied to compute the binding free energy (ΔG_{bind}). Van der Waals (ΔE_{vdW}) and gas-phase electrostatic (ΔE_{ele}) energies create the molecular mechanical term (ΔE_{MM}). A nonpolar (ΔG_{nonpol}) and polar (ΔG_{pol}) energies create ΔG_{solv}. The ΔG_{nonpol} was calculated using $\Delta G_{nonpol} = \gamma SASA + \beta$. The GBSA procedure of the AMBERTools16 was utilized to compute the G_{pol} [23]. The conformational entropy contribution ($-T\Delta S$) was estimated using the AMBER NMODE module [24].

2.4. Umbrella sampling simulation for ligand unbinding

In the late 20th century, umbrella sampling (US) approach was presented by Torrie and Valleau for the first time [25]. In brief, umbrella sampling includes using an umbrella biasing potential to limit sampling in a certain length of a reaction coordinate. To assess the potential of mean force (PMF) profiles, this method can generate a series of configurations, and in each initial configuration, MD simulations are applied by restraint-based configurational sampling surrounding some values of the desired reaction coordinate. Then, the weighted histogram analysis method (WHAM) was utilized to provide the favorable PMF curve along the reaction coordinate [25]. Finally, the $\Delta G_{bind/unbind}$ was calculated using the difference between the highest and lowest values of the PMF curve. In the selected windows, a force constant of 1000 kJ/mol.nm was applied. The US simulations were begun using the last conformations of the 50 ns conventional MD trajectories for both systems. For each system, US was done in a simulation box of dimensions $7.560 \times 7.362 \times 12$ nm. An umbrella biasing potential was applied to harmonically restrain the drug at increasing center-of-mass (COM) distance from protein. For drug unbinding, 48 windows were selected from the US simulations frames at distance intervals of 0.2 nm for both systems. In each window the temperature and the pressure were kept at 310 K and one atmospheric pressure by Nose–Hoover thermostat and Parrinello-Rahman barostat [26,27], during equilibration time (2 ns). Also, the main simulation time for each window was 10 ns. In total, MD simulation time was 480 ns for the US. The PMF plots estimated from the US simulations were convergent (Fig. S5).

3. Results and discussion

3.1. Molecular docking and MD simulation analyses

Docking analysis indicated that the T to S mutation slightly decreases the cefotaxime binding affinity to PBP1A (Table S1). Also, the analysis of docking complexes showed that there were some hydrogen-bonds between the drug and proteins (Fig. S3).

The MD simulations were begun by similar conformations of the PBP1A mutant and wild type variants, and the simulations were carried out for 60 ns on both systems. According to the root mean

squared deviations (RMSDs) of all backbone atoms of the wild type and mutant systems, both systems have achieved stability at the early times of simulations (Fig. 1a and Fig. S4a). However, the mutant system did have a larger RMSD than the wild type during MD simulations.

To study the effect of the mutation on the dynamics and conformations of the PBP1A binding pocket, RMSFs were calculated versus the residue numbers for PBP1A for the mutant and wild type states (Fig. 1c and Fig. S4b). The RMSF results showed that all the residues in the binding pocket (77–123 and 223–267) in the mutant PBP1A are more flexible compared with those sequences in wild type PBP1A during the simulation period (Fig. 1c). This high flexibility allows the cleft to be easily opened and the drug is rapidly released from the protein (Figs. S8a–e).

Since the point mutation of PBP1A was accompanied by a substantial conformation variation in the catalytic cleft, the backbone flexibility of the catalytic cleft of PBP1A might be essential for unbinding the cefotaxime. In fact, mutations at the conserved motifs on the catalytic cleft can affect the sensitivity of cefotaxime to the binding pocket by restricting its access through influencing the conformation or dynamics of the catalytic cleft. This confirms that the cefotaxime-resistant mutant's cleft opened more easily than the wild-type's cleft during the same simulation times.

3.2. *Antibiotic resistance mechanism defined using umbrella sampling*

As seen in Figs. 2f and 3g, the inhibitor left more easily the binding pocket of the mutant protein, suggesting that the T to S mutation can induce antibiotic resistance against cefotaxime.

According to the Fig. 2f, the minimum of the PMF value was stabilized with RC = ~1.3 nm. Afterwards, two different phases can be seen in the PMF diagram of the mutated complex during the unbinding process of the drug from the binding pocket: a rapid increase phase from 1.3 to 1.5 nm (Fig. 2f, a) and a steady but slower increase phase after 1.5–3.8 nm (Fig. 2f, b-d). The cefotaxime unbinding resulted in a decreased number of both H-bonds and contacts between cefotaxime and PBP1A (Fig. 2a–e). For the mutant complex, the total number of contacts reduced significantly from approximately 1100 to 200 at 1.8 nm along the reaction coordinates (Fig. 4). The reduced number of contacts mainly resulted from the breakage of interactions among the residues Y99, N100, W101, S156, N252, Y253, D255, and Q257 of PBP1A, and residues on the complementary subunit of the binding pocket (Figs. S6a–e). Besides reducing the number of interactions, unbinding of cefotaxime was also accompanied by breaking the H-bonds along the reaction coordinate (Fig. 2 a-e). The reduced number of contacts and H-bonds was responsible for the rapidly increased PMF of cefotaxime along the reaction coordinate (rapid increase phase) (Fig. 2f, a). Afterwards, the slope of the PMF became moderate (Fig. 2f, b-d). At 3.8 nm, the PMF of the mutant complex reached to plateaus, meaning that the cefotaxime is entirely dissociated from the mutant PBP1A (Fig. 2f, d-e).

The minimum of the PMF value is at a distance between the Center-of-Masses (COMs) of 1.52 nm (Fig. 3g). Afterwards, the PMF profile increases up to ~2.2 nm (Fig. 3g, a). In early stages of drug release, the hydrophobic and hydrogen bonds between the drug and some residues (Y99, N100, W101, S156, N252, Y253, D255, and Q257) are broken (Fig. 3a–f and 7Sa-f). In the next step, the PMF value increases slowly until the drug reaches to the entrance of the catalytic cleft (i.e., N250, N252, and Y253). In this position, the catalytic edges should be opened to allow the massive drug to pass (Fig. 3g, b-c), where the cefotaxime continually adjusts the posture to put up itself in the binding site (Fig. 3b–e or Figs. S7c–e). Afterwards, the PMF of the wild-type complex reached to plateaus, meaning that the cefotaxime is entirely released from the wild-type PBP1A (Fig. 3g, f).

In the early stages of drug release process, the PMF value of the mutated complex is greater than the wild-type complex (Fig. 2f), meaning that interactions between the drug and mutated protein are rapidly broken and the drug binding pocket collapses (Fig. 4a and b). Overall, According to WHAM analysis, the PMF value of the segregation of the drug from the wild-type protein is greater than the mutated protein (Figs. 2f and 3g). Consequently, the ΔG_{unbind} value of the drug/wild complex is higher than that of the drug/mutant complex, suggesting that the inhibitor can form relatively tighter interactions with the wild type PBP1A than with the mutant PBP1A.

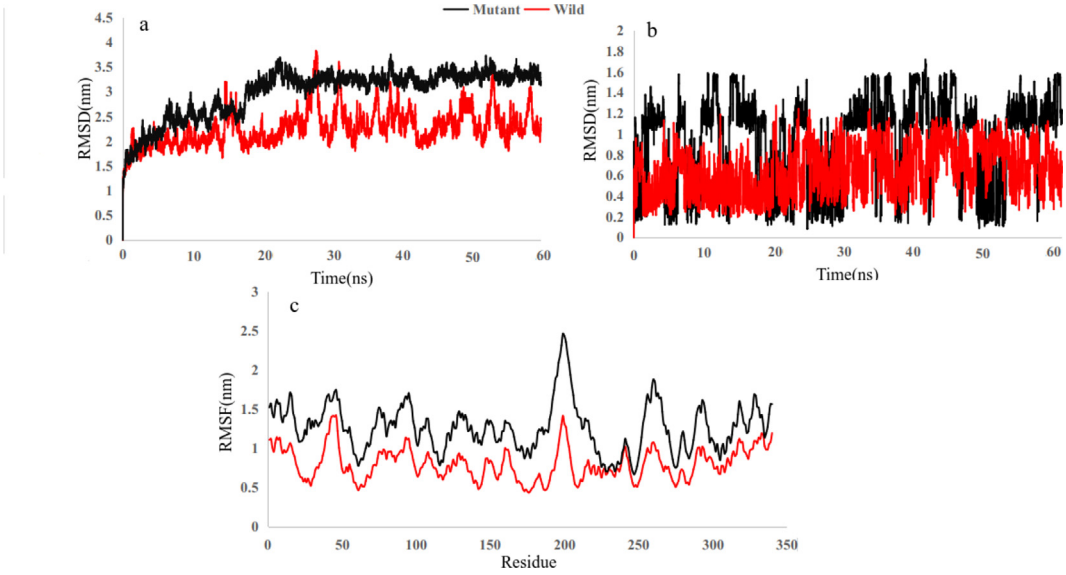

Fig. 1. Simulation outputs of cefotaxime-PBP1A complexes: (a) and (b) present the RMSD values of Cα for proteins and the RMSD values of heavy atoms of the drug in the complexes, respectively; (c) present the RMSF values of Cα atoms for the proteins.

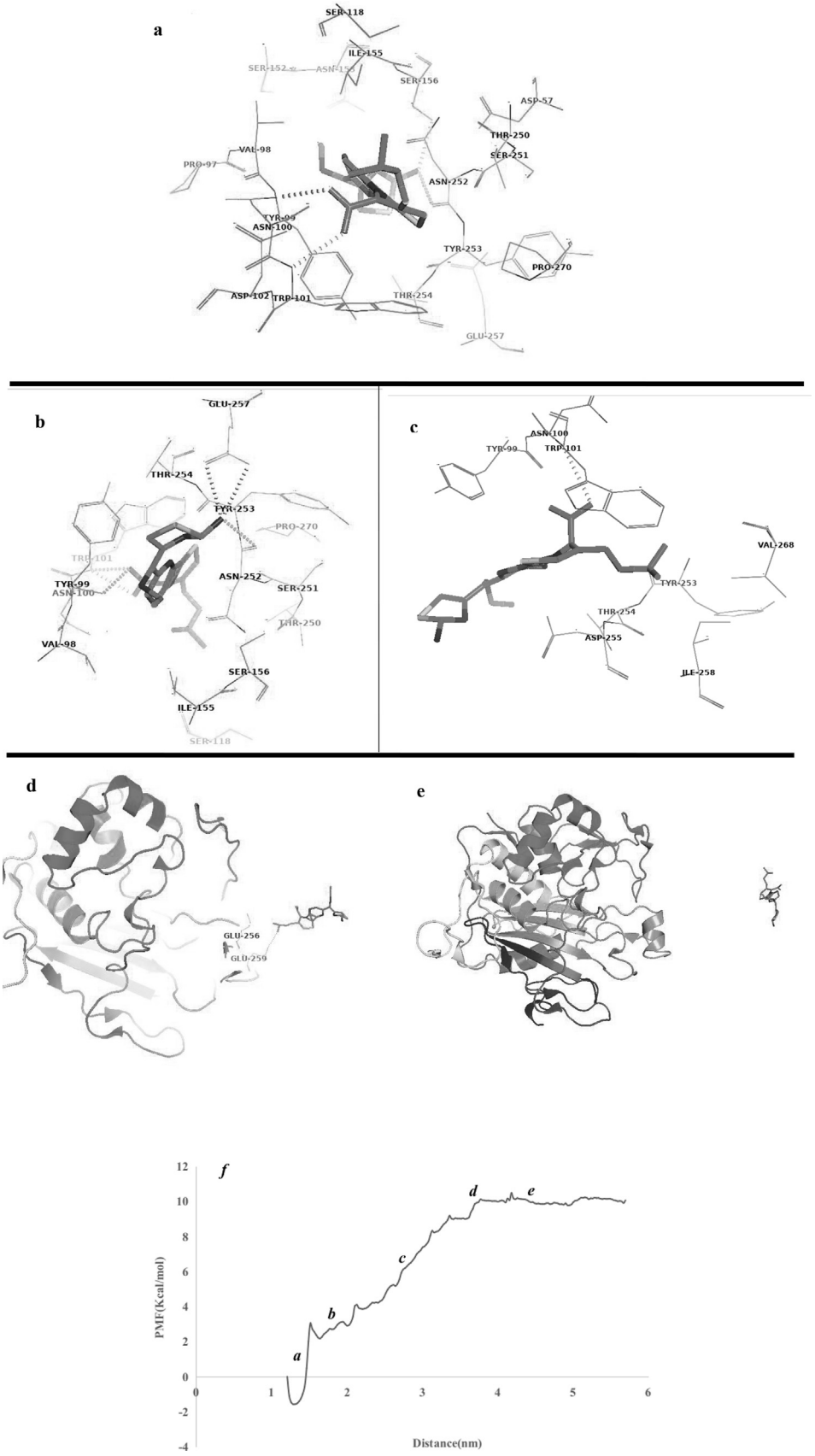

Fig. 2. Pulling cefotaxime from its bound state (mutant complex) to an unbound state (panels a–e); PMF profiles as a function of cefotaxime's displacement along the reaction coordinate (panel f). Yellow dotted lines represent hydrogen bond connections.

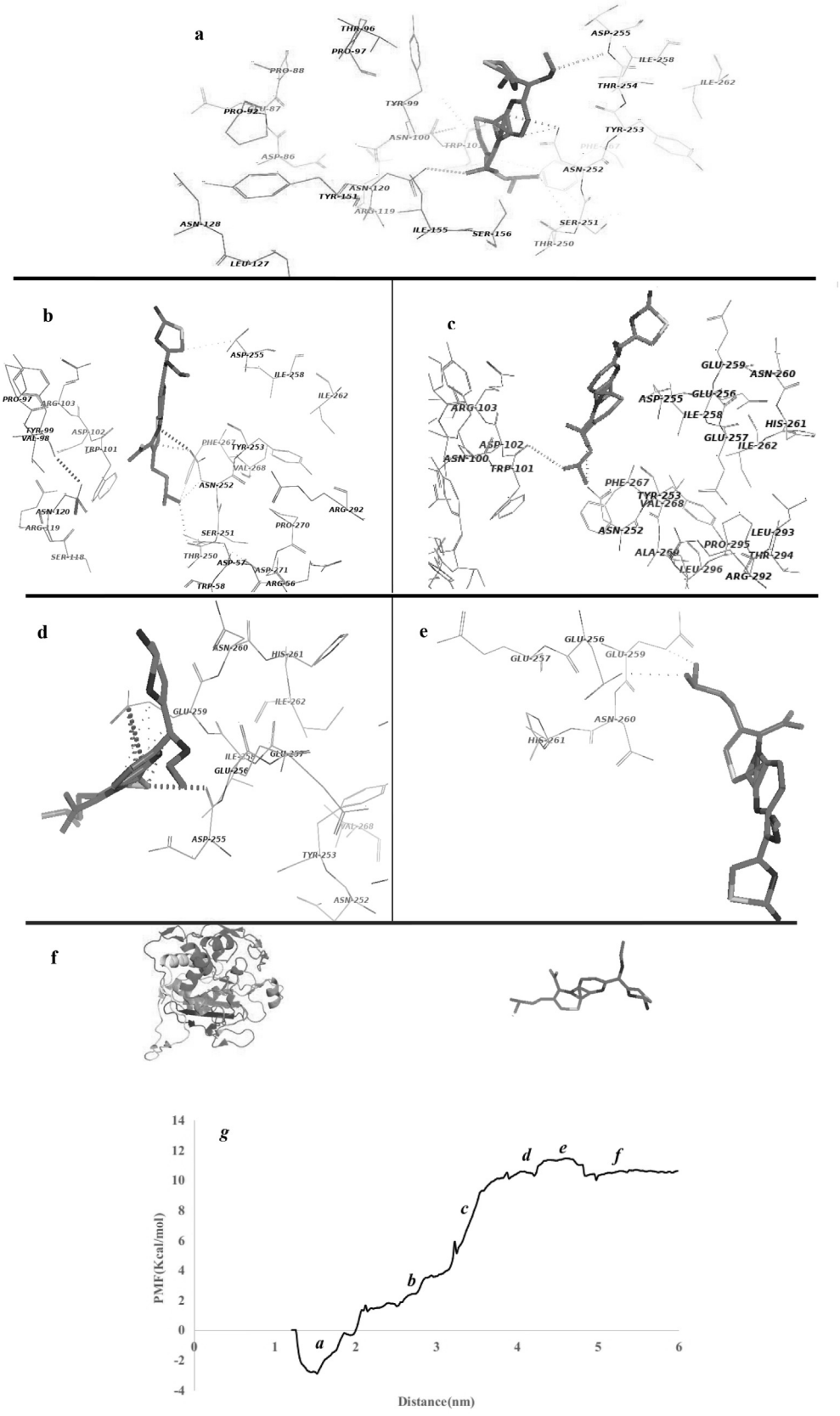

Fig. 3. Pulling cefotaxime from its bound state (wild type complex) to an unbound state (panels a–f); PMF profiles as a function of cefotaxime's displacement along the reaction coordinate (panel g). Magenta dotted lines represent hydrophobic interactions; yellow dotted lines represent hydrogen bond connections.

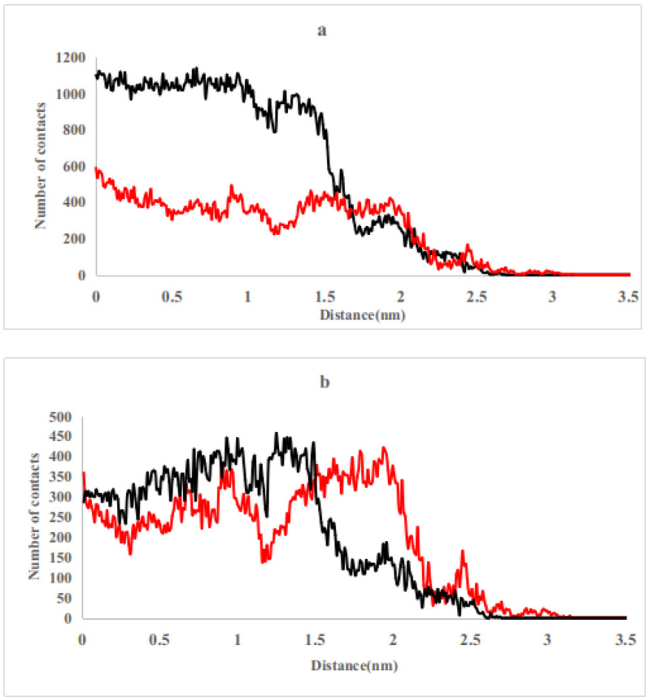

Fig. 4. (a) Variation of the number of contacts between cefotaxime and protein in the mutant (black line) and wild type (red line) complexes along the reaction coordinate; (b) Variation of the number of contacts between cefotaxime and residues 223–267 in the mutant (black line) and wild type (red line) complexes along the reaction coordinate. (For interpretation of the references to colour in this figure legend, the reader is referred to the Web version of this article.)

3.3. Binding free energy analysis

Table 1 shows that binding energy (ΔG_{bind}) of the mutated complex is less than that of the native complex, indicating that the drug binds more strongly to the wild type protein. Therefore, resistance to cefotaxime can result from the T to S mutation in the STMK conserved motif.

3.4. Effect of conformational entropy on the antibiotic resistance

Table 1 shows that the -TΔS value of the mutated complex is higher than that of the wild-type complex. Simulations analysis showed that the drug has a higher RMSD value in the mutant complex than the wild type complex (Fig. 1a and b). Moreover, compared to the native protein, the motifs 77–123 and 223–267 amino acids containing the drug binding pocket have a greater flexibility in the mutated protein. These areas include β-strand, loop, and α-helix structures (Fig. 1c). The high flexibility of the mutated complex represents high conformational changes in the binding pocket, which is consistent with the changes in the entropy value (-TΔS) in Table 1. In addition, the disappearance of interactions among some residues (W101, F267, and Y253) induces the instability in the α-helix, loop, and β-strand structures of the mutated PBP1A.

Table 1
The calculated binding free energy and the contribution of various energy components (kcal/mol).[a] Polar contribution of the solvation effect.[b] Non-polar contribution of solvation effect.[c] Enthalpic contribution.

	Wild	Mutant
ΔE_{ele}	−40.11 ± 0.41	−7.13 ± 0.28
ΔE_{vdW}	−54.98 ± 0.15	−40.93 ± 0.12
ΔG^{a}_{GB}	65.31 ± 0.35	25.53 ± 0.27
ΔG^{b}_{SA}	−5.67 ± 0.01	−4.22 ± 0.01
$\Delta E_{non\text{-}polar}$	−60.65 ± 0.15	−48.17 ± 0.12
ΔE_{polar}	25.20 ± 0.41	21.30 ± 0.28
$\Delta E^{c}_{enthalpy}$	−35.44 ± 0.15	−26.75 ± 0.12
-TΔS	9.5 ± 0.58	17.7 ± 0.71
ΔG_{bind}	−25.94 ± 0.37	−9.05 ± 0.42

3.5. Non-polar contacts are important to cefotaxime resistance

The contribution of all binding energy components is listed in Table 1. The enthalpy contribution for the wild type complex is −35.44 kcal/mol compared with −26.75 kcal/mol for the mutated complex. The polar contribution for the wild type and mutated complexes are 25.20 and 21.30 kcal/mol, respectively. Also, the non-polar contributions for the wild type and mutant complexes are −60.65 and −48.17 kcal/mol, respectively, meaning that the nonpolar term (hydrophobic contact) is a favorable contribution for drug binding to the protein, and the polar component plays an unfavorable role in the binding process. Therefore, it can be suggested that reducing the hydrophobic contacts and increasing the polar contribution in the binding energy play an important role in cefotaxime resistance.

Table 2 shows that the loop, β-strand, and α-helix regions of PBP1A contain the most key residues for the cefotaxime binding. Due to the Table 2, compared to the mutated complex, some of the hydrophobic residues (F267, W101, Y281 and Y253) in the wild-type complex have a dominant contribution in drug binding to create a strong hydrophobic contact with different elements of the drug (Fig. S11).

Thus, it can be suggested that hydrophobic contacts are the major driving force for drug binding to PBP1A. In addition, the reduction in the contribution of hydrophobic energies has an important role in reducing the affinity of the mutated protein to cefotaxime. Compared to the wild-type complex, the conformational changes in the binding pocket can lead to differences in the contacts between the drug and the mutated protein.

4. Conclusion

In conclusion, the results of MD simulations suggested that the T to S mutation reduces the stability of the conformation by destroying some important hydrophobic interactions in the catalytic cleft, which increases the flexibility of the catalytic cleft. In addition, the RMSF results showed that after the mutation, the binding pocket (especially residues 77–123 and 223–267) becomes more flexible. Thus, the catalytic cleft becomes more flexible in the mutated protein. As a result, during the same simulation time, the catalytic cleft opened more widely in the antibiotic-resistant mutant than the wild-type, and the drug comes more quickly out of it. All these factors reduce the affinity of the mutated protein to the drug or cause the binding capacity to weaken

Table 2
The contribution of key residues in the ΔG_{bind} (kcal/mol).

Name	Wild type	Mutant
W101	−3.35	0.22
Y250	−1.7	0.07
N252	−1.34	0.20
Y253	−2.13	0.1
I258	−1.82	0.06
F267	−5.39	−1.4
V268	−2.19	0.3
Y281	−4.9	−0.003

between the drug and the protein, and the drug can quickly separate from the protein. The usage of computational techniques to clarify antibiotic resistance in bacterial infections is important, rapid, and beneficial. Consequently, the data provided by this study can help design new agents with high inhibitory potential against bacterial infections.

Appendix A. Supplementary data

Supplementary data to this article can be found online at https://doi.org/10.1016/j.jmgm.2018.12.002.

References

[1] F. Baquero, J. Blàazquez, Evolution of antibiotic resistance, Trends Ecol. Evol. 12 (1997) 482–487.
[2] E. Abebe, B. Tegegne, S. Tibebu, A review on molecular mechanisms of bacterial resistance to antibiotics, EJAS 8 (2016) 301–310.
[3] K. Bush, A resurgence of β-lactamase inhibitor combinations effective against multidrug-resistant Gram-negative pathogens, Int. J. Antimicrob. Agents 46 (2015) 483–493.
[4] X.-Z. Li, H. Nikaido, Efflux-mediated drug resistance in bacteria, Drugs 64 (2004) 159–204.
[5] B.H. Normark, S. Normark, Evolution and spread of antibiotic resistance, J. Intern. Med. 252 (2002) 91–106.
[6] B. Beovic, The issue of antimicrobial resistance in human medicine, Int. J. Food Microbiol. 112 (2006) 280–287.
[7] L. Fernandez, R.E. Hancock, Adaptive and mutational resistance: role of porins and efflux pumps in drug resistance, Clin. Microbiol. Rev. 25 (2012) 661–681.
[8] K.P. Langton, P.J. Henderson, R.B. Herbert, Antibiotic resistance: multidrug efflux proteins, a common transport mechanism? Nat. Prod. Rep. 22 (2005) 439–451.
[9] K. Poole, Efflux-mediated antimicrobial resistance, J. Antimicrob. Chemother. 56 (2005) 20–51.
[10] A. Zapun, C. Contreras-Martel, T. Vernet, Penicillin-binding proteins and beta-lactam resistance, FEMS Microbiol. Rev. 32 (2008) 361–385.
[11] F. Ikeda, Y. Yokota, A. Ikemoto, N. Teratani, K. Shimomura, H. Kanno, Interaction of beta-lactam antibiotics with the penicillin-binding proteins of penicillin-resistant Streptococcus pneumoniae, Chemotherapy 41 (1995) 159–164.
[12] P. Macheboeuf, C. Contreras-Martel, V. Job, O. Dideberg, A. Dessen, Penicillin binding proteins: key players in bacterial cell cycle and drug resistance processes, FEMS Microbiol. Rev. 30 (2006) 673–691.
[13] E. Sauvage, F. Kerff, M. Terrak, J.A. Ayala, P. Charlier, The penicillin binding proteins: structure and role in peptidoglycan biosynthesis, Microbiol. Rev. 32 (2008) 556, 556.
[14] V. Job, R. Carapito, T. Vernet, A. Dessen, A. Zapun, Crystal structure of PBP1A from drug-resistant strain 5204 from Streptococcus pneumoniae, J. Biol. Chem. 283 (2007) 4886–4894.
[15] Y. Ghouzam, G. Postic, A.G. de Brevern, J.C. Gelly, Improving protein fold recognition with hybrid profiles combining sequence and structure evolution, Bioinformatics 31 (2015) 3782–3789.
[16] G.M. Morris, R. Huey, W. Lindstrom, M.F. Sanner, R.K. Belew, D.S. Goodsell, A.J. Olson, AutoDock4 and AutoDockTools4: automated docking with selective receptor flexibility, J. Comput. Chem. 30 (2009) 2785–2791.
[17] O. Trott, A.J. Olson, AutoDock Vina: improving the speed and accuracy of docking with a new scoring function, efficient optimization, and multithreading, J. Comput. Chem. 31 (2010) 455–461.
[18] U. Essmann, L. Perera, M.L. Berkowitz, T. Darden, H. Lee, L.G. Pedersen, A smooth particle mesh ewald potential, J. Chem. Phys. 103 (1995) 8577–8592.
[19] J.P. Ryckaert, G. Ciccotti, H.J.C. Berendsen, Numerical integration of the cartesian of motion of a system with constraints: molecular dynamics of n-alkanes, J. Comput. Phys. 23 (1977) 327–341.
[20] B. Hess, H. Bekker, H.J.C. Berendsen, J.G.E.M. Fraaije, LINCS: a linear constraint solver for molecular simulations, J. Comput. Chem. 18 (1997) 1463–1472.
[21] L. Schrodinger, The AxPyMOL Molecular Graphics Plugin for Microsoft PowerPoint, Versioñ1.0, 2010.
[22] C. Wallace, A. Laskowski, J.M. Thornton, LIGPLOT: a program to generate schematic diagrams of protein–ligand interactions, Protein Eng. 8 (1995) 127–134.
[23] M. Levitt, C. Sander, P.S. Stern, Protein normal-mode dynamics trypsin inhibitor, crambin, ribonuclease and lysozyme, J. Mol. Biol. 181 (1985) 423–447.
[24] G. Rastelli, A.D. Rio, G. Degliesposti, M. Sgobba, Fast and accurate predictions of binding free energies using MMPBSA and MMGBSA, J. Comput. Chem. 31 (2010) 797–810.
[25] J.S. Hub, B.L. De Groot, D. Van der Spoel, g_wham-A free weighted histogram analysis implementation including robust error and autocorrelation estimates, J. Chem. Theor. Comput. 6 (2010) 3713–3720.
[26] M. Parrinello, R. Aneesur, Polymorphic transitions in single crystals: a new molecular dynamics method, J. Appl. Phys. 52 (1981) 7182–7190.
[27] S. Nosé, M.L. Klein, Constant pressure molecular dynamics for molecular systems, Mol. Phys. 50 (1983) 1055–1076.